ELSEVIER

Computational Materials Science 8 (1997) 107–121

MATERIALS SCIENCE

Ni–Au: A testing ground for theories of phase stability

C. Wolverton *, Alex Zunger

National Renewable Energy Laboratory, Golden, CO 80401, USA

Abstract

The theory of phase stability in the Ni–Au alloy system is a popular topic due to the large size mismatch between Ni and Au, which makes the effects of atomic relaxation critical and also to the fact that Ni–Au exhibits a phase separation tendency at low temperatures, but measurements at high-temperature show an ordering-type short-range order. We have [illegible] properties by computing state-of-the-art energetics (full-potential, fully relaxed LDA total energies) combined with 'state-of-the-art' statistics (*k*-space cluster expansion with Monte Carlo simulations) for the Ni–Au system. We find: (i) LDA provides accurate mixing energies of disordered $Ni_{1-x}Au_x$ alloys ($\Delta H_{mix} \leq +100$ meV/atom) provided that both atomic relaxation (a ~100 meV/atom effect) and short-range order (a ~25 meV/atom) are taken into account properly. (ii) [illegible] entropy of mixing combined with calculated values of the configurational entropy demonstrate that the non-configurational entropy in Ni–Au is large and leads to a significant reduction in miscibility gap temperature. (iv) The calculated short-range order agrees well with measurements and both predict *ordering* in the disordered phase. (v) Consequently, using inverse Monte Carlo to extract interaction energies from the measured/calculated short-range order in Ni–Au would result in interactions which would produce ordering-type mixing energies, in contradiction with both experimental measurements and precise LDA calculations.

1. Introduction

The Ni–Au alloy system is physically interesting because it exhibits on the one hand a phase separation tendency at low temperatures and positive mixing enthalpies [1] and on the other hand exhibits at high temperatures an ordering-type short-range order [illegible] peak intensity away from the Γ-point, despite the fact that phase-separating systems are expected to

* Corresponding author. E-mail: cmw@sst.nrel.gov.

PII S0927-0256(97)00023-2

show a peak at Γ.[1] Also, the fcc Ni and Au constituents possess a large lattice mismatch ($\Delta a/a \sim 15\%$), thus making this system a critical test for any alloy phase stability theory hoping to capture the effects of atomic relaxation. Important early experimental and theoretical work on this alloy includes [illegible] Cook and de Fontaine [7]. The coexistence of phase separation (at low T) with short-range ordering (at high T) in the same alloy system might have been ('anti-ferromagnetic') interactions at higher T. The change would have been surprising, given that no electronic, magnetic, or structural change is observed in this temperature range. The answer to this puzzle was given by Lu and Zunge [8]: The excess energy for a disordered $Ni_{1-x}Au_x$ alloy or an ordered compound with configuration of type σ is given by:

$$\Delta H_\sigma = E_\sigma\left(a_{eq}^\sigma\right) - \left[(1-x)E_{Ni}\left(a_{eq}^{Ni}\right) + xE_{Au}\left(a_{eq}^{Au}\right)\right], \quad (1)$$

and may be written [9] $\Delta H = \Delta\epsilon + \Delta E_{VD}$, where $\Delta\epsilon$ is the constant-volume, 'spin-flip' energy required to create the configuration σ out of Ni and Au, each already prepared at the alloy lattice constant a_{eq}^σ and ΔE_{VD} is the volume deformation energy required to hydrostatically deform Ni and Au from their respective lattice parameters a_{eq}^{Ni} and a_{eq}^{Au} to a_{eq}^σ. In Ref. [8], it is demonstrated that SRO is determined by the constant-volume energy change $\Delta\epsilon$, which is negative (ordering, or 'anti-ferromagnetic') in Ni–Au, indicating an ordering tendency of SRO. However, $\Delta E_{VD} = G(x)$ is large and positive, making $\Delta H > 0$. And, since long-range order is [illegible] ('ferromagnetic') long-range order. This analysis leads to two unexpected conclusions: first, that the time-honored Ising-like representation of alloy thermodynamics [illegible] will fail to explain basic stability trends for systems such as Ni–Au. Second, since measurements or calculations of the SRO are insensitive to physical effects (i.e. elastic deformation ΔE_{VD}) that control measurements/calculations of mixing enthalpies ΔH, the often-used practice (see e.g. Ref. [10–13] of 'inverting' the SRO profile to extract interaction energies that are then used to predict mixing enthalpies is *fundamentally flawed*. Specifically, inversion of the SRO of Ni–Au will produce ordering-like interaction energies which, when used to calculate mixing enthalpies, will produce (ordering-like) negative values, while the measured ones are strongly positive [1,14].

For these and other reasons, theoretical investigations of phase stability in Ni–Au have recently become quite popular [8,15–22] (Table 1). These calculations are distinguished by the methods used for (i) [illegible] ($T = 0$ K) and (ii) statistics ($T > 0$). Energy calculations ($T = 0$ K) for this system have been performed by a wide variety of techniques: [illegible] approximation (LMTO [16–18] and ASW [19]), as well as semi-empirical (EAM [20]) and empirical [illegible] in the computed energetics (Table 1). Statistics have been applied to these calculations using cluster expansions (CE) such as ϵ–G [9], Connolly-Williams [illegible]

The purpose of this paper is thus three-fold:

First, we would like to clarify the conflicting energetic and statistical results (Table 1) by computing 'state-of-the-art' energetics for Ni–Au alloys (full-potential LAPW total energies including full atomic relaxation) combined with 'state-of-the-art'

[illegible]

simulation, they noted clusters of Ni atoms, with the wavelength of these clusters corresponding to the peak of the measured SRO pattern in reciprocal space, a_{SRO} (0,0, 0,0). These facts indicate a short-range *clustering* tendency along the (100) direction. Although our calculations agree with these observations, there appears to be a semantic problem of how to characterize these facts. When considering all of the measured data, we classify the Cowley SRO parameters in real-space show strong negative (ordering-type) values in many shells *other* than second neighbor, indicating that the clustering tendency in the second shell is competing with an ordering tendency in many other shells. (2) The total SRO pattern in reciprocal space (including 20 real-space shells) shows peaks *away* from the Γ-point, the typical wavevector for clustering-type tendencies.

Table 1

Summary of energy calculations performed for $Ni_{1-x}Au_x$ alloys. Shown are the methods used to compute $T = 0$ energetics, as well as the type of cluster expansion (CE) and statistics used. Also given is the mixing energy of the $T \to \infty$ random alloy near $x = 1/2$ and the calculated miscibility gap temperature, if available. FLAPW = full-potential linearized augmented plane wave method, FLMTO = full-potential linear muffin-tin orbital method, ASW = augmented spherical wave method, LMTO-ASA = linear muffin-tin orbital method in the SOE = second-order expansion

Authors	$T = 0$ energy	Method		Results	
		cluster expansion technique	statistics	ΔH_{mix}^{fcc}	T_{MG} (K)
Wolverton and Zunger [a]	FLAPW	**k**-space CE	MC	+118	
Lu and Zunger [b]	FLAPW	ϵ-G	MC	+127	
Deutsch and Pasturel [c]	FLMTO	ϵ-G	none	+136	
Takizawa, Terakura, and Mohri [d]	ASW	CW	CVM	+170	
Amador and Bozzolo [e]	LMTO-ASA	CW	CVM	+150	
Colinet et al. [f]	LMTO-ASA	ϵ-G	CVM	+67	1200-1400
Morgan and de Fontaine [g]	LMTO-ASA + 'Elastic Springs'	ϵ-G	CVM	+98	2330
Eymery et al. [h]	empir. potential	simulation	none	+60	
Tetot and Finel [i]	empir. potential	simulation	MC	+48 [m]	950
Deutsch and Pasturel [c]	empir. potential	simulation	none	+83	
Asta and Foiles [j]	EAM	SOE	MC/MF	+78	2460
Expt. (calorimetry) $T = 1150$ K [k]				+76	
Expt. (EMF) $T = 1173$ K [l]				+77	
Expt. (phase diagram)					1083

statistics (a k-space CE [25] with Monte Carlo simulations). These computations will clarify whether the better agreement with experimental ΔH obtained by approximated methods (e.g. empirical and semi-empirical potentials, as well as atomic-sphere-approximation methods) relative to full LDA methods is fundamental or accidental.

Second, we would like to address the issue of why the calculated miscibility gap temperatures are often much too high compared with the experimen-

see a fixed ratio between calculated miscibility gap temperatures T_{MG} and the calculated ΔH_{mix}. In fact, all previous calculations (except the EAM calculations of Asta and Foiles [20]) very nearly follow the

trony: $k_B T_{MG}/\Delta H_{mix} = 2$. However, the *experimen-*

apparent discrepancy between experimental ΔH_{mix} and T_{MG} below.

Third, we would like to examine the SRO in Ni–Au and discuss the implications of this SRO on

ing phase stability in alloys. We will offer a challenge to practitioners of the inverse Monte Carlo method.

2. Checking ordered compound formation energies

Table 1 summarizes the results of previous calculations on the mixing enthalpies of random Ni–Au alloys. The wide discrepancy between calculated values of ΔH_{mix} (48–170 meV/atom) is apparent from

alloys can be expressed (see e.g. Eq. 3b in Ref. [26]) as a linear combination of formation enthalpies $\Delta H_f(\sigma)$ of certain ordered compounds $\{\sigma\}$, the discrepancies in ΔH_{mix} must reflect discrepancies in $\Delta H_f(\sigma)$. Put formation enthalpies of small unit cell ordered compounds can be computed accurately and

ods. Our strategy will thus be to trace the source of the discrepancy in ΔH_{mix} to the values of formation energies of various Ni_pAu_q ordered compounds, as shown in Table 2. Examining this table leads to

Ni–Au.

Table 2
Comparison of formation enthalpies $\Delta H(\sigma)$ for Ni–Au ordered compounds. Nomenclature for the ordered structures is the same as that

Structure	Fully relaxed FLAPW [a]	Partially relaxed FLAPW [b]	FLMTO [c]	ASW [d]	LMTO [e]	Empirical potential [c]	EAM [j]
[illegible]	[illegible]	[illegible]	[illegible]	[illegible]	[illegible]	[illegible]	[illegible]
NiAu ($L1_1$)	+166.8 (+192.3)	+167.6	+175.4		(+177.9)		+72.9 (+159.7)
NiAu ('40')	+84.8 (+93.5)	+83.8	+89.9		(+114.3)		−1.9 (+96.4)
Ni_3Au ($L1_2$)	+77.5	+75.5	+80.7	+42	+92.4	+58.1	+77.1
Ni_3Au ($D0_{22}$)	+75.0 (+75.0)		+81.5		(+95.3)		
[illegible]	[illegible]	[illegible]	[illegible]	[illegible]	[illegible]	[illegible]	[illegible]
$NiAu_3$ ($D0_{22}$)	+68.6 (+68.7)		+68.0		(+76.4)		

[a] Present results. Complete atomic relaxation via quantum mechanical forces and total-energy minimization.
[b] Ref. [8]. Partial atomic relaxation via continuum elasticity, using Eqs. (2)–(6).
[c] Ref. [15].
[d] [illegible]
[e] Ref. [18]. LMTO-ASA with sphere radii chosen to minimize charge transfer.
[j] Ref. [20].

2.1. FLMTO versus ASA methods (LMTO, ASW)

In comparing the full-potential LMTO [15] to LMTO-ASA [18] calculations, one can see significant differences, even when considering unrelaxed configurations. For example, the $Z2$ structure (a Ni_2Au_2 (001) superlattice) has an unrelaxed formation energy which is nearly 100 meV/atom lower in the LMTO-ASA calculation than in the full-potential LMTO one. Thus, the ASA-based calculations (LMTO, ASW) in the Ni–Au system cannot be relied upon for the kind of quantitative energetics required in phase stability studies (for a list of many cases in which ASA and full-potential formation energies significantly disagree see Table 1 in Ref. [27]).

2.2. Harmonic versus anharmonic relaxation

In a large lattice-mismatched system like Ni–Au, the effects of atomic relaxation are likely to be crucial. Although straightforward, fully relaxing all of the cell-internal and cell-external degrees of freedom can be computer intensive. One alternative to full atomic relaxation (using quantum mechanical forces and total energy minimization) which has [illegible] theory [28] to find the relaxed geometry, with a subsequent LDA calculation with this geometry to find the relaxed energetics. Continuum elasticity theory can be used as a relaxation model by realizing

scribed as 'superlattices' along some special orientations $\hat{k}$. Continuum elasticity then provides the equilibrium interlayer spacing c_{eq} along $\hat{k}$ as a function of the externally-fixed perpendicular lattice constant $a_\perp$ as the minimum of the epitaxial strain energy due to the external constraint:

$$c_{eq}(\hat{k}, a_\perp) = a_{eq}^{(\lambda)} + [2 - 3q^{(\lambda)}(a_\perp, \hat{k})][a_{eq}^{(\lambda)} - a_\perp] + \ldots \quad (2)$$

$$q(a_\perp, \hat{k}) = \frac{\Delta E_{epi}^{eq}(a_\perp, \hat{k})}{\Delta E_{bulk}(a_\perp)} \quad (3)$$

where $E_{eq}^{(\lambda)}$ and $a_{eq}^{(\lambda)}$ are the equilibrium energy and lattice constant of the cubic material λ. ΔE_{epi}^{eq} is the energy of the alloy constituent subject to he biaxial constraint that the lattice constant perpendicular to $\hat{k}$ be externally fixed at $a_\perp$. $\Delta E_{bulk}(a_\perp)$ is simply the deformation energy change upon hydrostatically distorting the material from a_{eq} to $a_\perp$. The central

reduction factor' $q(a_\perp, \hat{k})$. In continuum elasticity theories, $q(a_\perp, \hat{k})$ is given by

$$q(a_\perp, \hat{k}) = 1 - B/[C_{44} + \alpha(a_\perp, \hat{k})A] \quad (4)$$

$$A = C_{44} - (C_{11} - C_{12})/2 \quad (5)$$

is the elastic anisotropy, $B = (C_{11} + 2C_{12})/3$ is the bulk modulus and C_{ij} are elastic constants. In the harmonic approximation, $q(a_\perp, \hat{k})$ is further assumed to be $a_\perp$-independent and $\gamma_{\text{harm}}(\hat{k})$ is the following geometric function for the direction $\hat{k} = (l, m, n)$:

$$\gamma_{\text{harm}}(l, m, n) = \frac{4(l^2m^2 + m^2n^2 + n^2l^2)}{(l^2 + m^2 + n^2)^2}$$

$$= \frac{4}{5}\sqrt{4\pi}\left[K_0(l, m, n) - \frac{\sqrt{70}}{8}K_4(l, m, n)\right]$$

where K_L are the Kubic harmonics of angular momentum L.

Using Eqs. (2)–(6) thus provides predicted relaxed geometries $c_{\text{eq}}(\hat{k}, a_\perp)$ for alloy compounds (e.g. the $Z2$ structure) given the elastic constants and $a_{\text{eq}}^{(\lambda)}$. Indeed, these equations have been routinely used (see review in Ref. [29]) to predict the distortion $c_{\text{eq}} - a_{\text{eq}}$ of films grown epitaxially on a substrate with lateral lattice constant $a_\perp$. Comparison to LDA calculations [30] shows that for semiconductors with lattice mismatch $(a_{\text{eq}} - a_\perp)/a_\perp \lesssim 7\%$, the harmonic expressions (Eqs. (4)–(6)) work very well down to a monolayer thickness. However, we find that for noble- and transition-metal alloys with a [illegible] misfit, anharmonic corrections are important. As we will see below in [illegible] of Eq. (4) now has additional terms to those appearing in the harmonic form of Eq. (6). These anharmonic terms in $\gamma(\hat{k})$ lead via Eq. (4) to corrections to $q(a_\perp, \hat{k})$ and consequently via Eq. (2) to the relaxation of the lattice constant $c_{\text{eq}}(\hat{k})$. Indeed, using [illegible] in Table 2) rather than via the harmonic expression of Eq. (4) ('partially relaxed' in Table 2), we find a lower-energy relaxation for $Z2$: The LDA energy minimization gives $\Delta H(Z2) = +70.2$ meV/atom, [illegible] theless, anharmonic relaxation in Ni–Au alloys is large and cannot be neglected.

2.3. Empirical methods: Getting the right $\Delta H_{mix}(x, T)$ for the wrong reason?

We see from Table 1 that the methods that use empirical evaluations of $\Delta H_{\text{mix}}(1/2, \infty)$ [15,18,20–22] produce results that are lower and thus closer to the measured $\Delta H_{\text{mix}}(1/2, 1150)$ than methods that use converged, full potential, fully relaxed approaches (i.e. the present work and Refs. [8,15]). Since there is a proportionality between ΔH_{mix} and $\Delta H(x_2)$, we surmise that the empirical methods will produce formation energies $\Delta H(x_2)$ of ordered [illegible] such systems. Indeed, Table 2 shows the formation energies of two of the empirical potential methods. By comparing these numbers to full-potential LDA energies, one can see that the *empirical potentials systematically underestimate the formation energies of ordered compounds*. Since the LDA method is expected to reproduce formation enthalpies of small-unit-cell ordered structures rather accurately and since FLAPW gives a precise representation of the LDA, we think that the underestimation of FLAPW energies by the empirical methods is a rather serious limitation of these methods. The EAM of Ref. [20] was fit to the unrelaxed FLAPW calculations of Ref. [8] and thus reproduces these energies fairly well (except for the $Z2$ structure). However, [illegible] of relaxation and hence produces relaxed formation energies which are much lower than LDA and [illegible] able to see more formation energies of ordered com-

[2] The Ni–Au system is especially difficult for the EAM. Simi- [illegible] [31].

expectation of underestimation of $\Delta H_f(\sigma)$ relative to LDA.

In summary, the reason that empirical methods agree with measured random-alloy mixing enthalpy

mation by the empirical methods of even the ordered

3. Present calculations: FLAPW with *k*-space cluster expansion

3.1. FLAPW calculations of ordered compounds

We have performed first-principles full-potential

Table 3
Listing of the LAPW calculated unrelaxed and relaxed $\Delta H(\sigma)$ (in meV/atom) for $Ni_{1-x}Au_x$. Many of the structures calculated here can

AB	$L1_0$	$L1_0$	$L1_0$	$L1_1$	$L1_1$
Unrelaxed	+98.1	+98.1	+98.1	+192.3	+192.3
Relaxed	+76.1	+76.1	+76.1	+166.8	+166.8
CE (relaxed)	+74.8	+74.8	+74.8	+167.1	+167.1
A_2B	$\beta 1$	$\gamma 1$		$\alpha 1$	
Unrelaxed	+207.8	+123.3		+288.5	
Relaxed	+105.7	+98.9		+202.2	
CE (relaxed)	+105.9	+102.4		+208.4	
Unrelaxed					
Relaxed	+38.3	+102.6		+100.9	
CE (relaxed)	+37.8	+98.8		+94.5	
A_3B	$Z1$	$Y1$	DO_{22}	$V1$	$W1$
Unrelaxed	+221.7	+148.5	+75.0	+290.8	
Relaxed	+89.9	+99.2	+75.0	+193.7	+125.7
Unrelaxed	+142.0	+104.1	+68.7	+172.8	
Relaxed	+32.4	+78.7	+68.6	+83.0	+88.4
CE (relaxed)	+28.2	+77.7	+67.6	+79.1	+83.2
A_2B_2	$Z2$	$Y2$	'40'	$V2$	$W2$
Unrelaxed	+286.7	+192.3	+93.5	+335.8	+144.2
Relaxed	+70.2	+96.6	+84.8	+162.4	+93.6
CE (relaxed)	+69.9	+101.1	+88.3	+166.7	+99.3
A_pB_p $(p \to \infty)$					
Unrelaxed	+576.2	+576.2	+576.2	+576.2	+576.2
CE (relaxed)	+30.8	+116.1	+86.8	+172.5	+117.9
Other structures					
	$L1_2$ (A_3B)	$L1_2$ (AB_3)	D7 (A_7B)	$D7_b$ (A_7B)	
Unrelaxed	+77.5	+78.9	+82.9	56.8	
Relaxed	+77.5	+78.9	+82.9	56.8	
CE (relaxed)	+80.7	+78.6	+98.5	57.6	
	$SQS14_a$ (A_6B_2)	$SQS14_b$ (A_2B_6)	Z6 (A_3B_3-100)	Z5 (A_2B_3-100)	
Unrelaxed	+183.2	+118.2	+355.5	+273.3	
Relaxed	+96.8	+59.8	+63.2	+57.1	
CE (relaxed)	+81.5	+75.0	+62.5	+57.9	

large number (31) of fcc-based Ni–Au compounds in order to construct an accurate cluster expansion. The total energy of each compound is fully minimized

We have used the exchange correlation of Wigner [33]. The muffin-tin radii are chosen to be 2.2 a.u. for Ni and 2.4 a.u. for Au. Brillouin-zone integrations are performed using the equivalent k-point

compound all mapping into the same 60 special k-points for the fcc structure. This mapping guarantees that the total energy per atom of an elemental metal calculated either with the fcc unit cell or with a lower symmetry (e.g. any of the compounds) are identical. All calculations performed are non-mag-

and found to be -50 meV/atom.)

The 31 calculated LAPW formation energies are given in Table 3. Both relaxed and unrelaxed (total

cell-internal and cell-external coordinates held fixed at ideal fcc positions) formation energies are shown. The nomenclature of the compounds studied is the same as given in Ref. [26]. Many of the compounds considered can be described as Ni_pAu_q 'superlattices' along a particular orientation k:

Ni_1Au_1: [100], [111],

Ni_2Au_1: [100], [011], [111],

Ni_2Au_2: [100], [011], [201], [111], [311],

Ni_3Au_3: [100],

We also calculated the energies of six other structures: $L1_2$(Ni_3Au and $NiAu_3$), D7(Ni_7Au and $NiAu_7$) and two 8-atom 'special quasi-random struc-

$q \to \infty$) needed in the construction of the k-space cluster expansion (see below) were computed for six principal directions: [100], [011], [201], [111], [311] and [221]. The numerical error of the LAPW calculations of ΔH_f is estimated to be

less.

3.2. k-space cluster expansion

The Ni–Au formation energies ΔH_σ for structures σ are then mapped onto a cluster expansion using the k-space formulation of Laks et al. [3],

expand with respect to a reference energy:

$$\Delta E_{\mathrm{CE}}(\sigma) = \Delta H^{\mathrm{LDA}}(\sigma) - E_{\mathrm{ref}} \tag{8}$$

We will separate the CE into two parts: (i) the terms

aration will be conveniently summed using the reciprocal space concentration-wave formalism and (ii) all terms but the pairs will be cast in real-space:

$$\Delta E_{CE}(\sigma) = \sum_{\boldsymbol{k}} J(\boldsymbol{k}) |S(\boldsymbol{k}, \sigma)|^2 + \sum_f D_f J_f \overline{\Pi}_f(\sigma) \tag{9}$$

The first summation includes all pair figures and the

the reciprocal space summation in Eq. (9), $J(k)$ and

real-space pair interactions and spin-occupation variables, J_{ij} and $\hat{S}_{ij}$, respectively, and the spin-occupation variables take the value $\hat{S}_i = -1(+1)$, denoting

integral of the gradient of $J(\boldsymbol{k})$. The real-space summation of Eq. (9) is over f, the symmetry-distinct non-pair figures (points, triplets, etc.), D_f is the

interaction for the figure f and Π_f is a product of the variables $\hat{S}_i$ over all sites of the figure f, aver-

sites.

[3] Generally, it was found that relaxing the cell-internal degrees

For some low-symmetry monoclinic structures relaxation of the length of the unit cell vectors provided an insignificant amount of

variation of the angle of the unit cell vectors was neglected.

The reference energy of Eq. (8) is chosen to contain infinite-range real-space elastic interaction

$$E_{\mathrm{ref}} = \frac{1}{4x(1-x)} \sum_{k} \Delta E_{\mathrm{CS}}^{\mathrm{eq}}(k, x)|S(k, \sigma)| \quad (10)$$

where $\Delta E_{\mathrm{CS}}(k, x)$ is the equilibrium constituent

dicular to k. $\Delta E_{\mathrm{CS}}^{\mathrm{eq}}(k, x)$ can thus be written as the minimum of the following expression with respect to $a_\perp$

$$\Delta E_{\mathrm{CS}}^{\mathrm{eq}}(\hat{k}, x) = (1-x) q^{\mathrm{Ni}}(a_\perp, k) \Delta E_{\mathrm{bulk}}^{\mathrm{Ni}}(a_\perp) + x q^{\mathrm{Au}}(a_\perp, \hat{k}) \Delta E_{\mathrm{bulk}}^{\mathrm{Au}}(a_\perp) \quad (11)$$

where $q^{(\lambda)}(a_\perp, \hat{k})$ is given by Eq. (2).

The final expression used for the formation energy of any configuration σ is then

$$\Delta H(\sigma) = \sum_{k} J(k)|S(k, \sigma)|^2 + \sum_{f} D_f J_f \overline{\Pi}_f(\sigma) + \frac{1}{4x(1-x)} \sum_{k} \Delta E_{\mathrm{CS}}^{\mathrm{eq}}(\hat{k}, x)|S(k, \sigma)|^2 \quad (12)$$

The following *input* is needed to construct this

ergy of any fcc-based configuration (i.e. not only

3.3. Anharmonic calculation of constituent strain

Laks et al. [25] demonstrated that the calculation of $\Delta E_{\mathrm{CS}}^{\mathrm{eq}}(\hat{k}, x)$ of Eq. (11) is significantly simplified if one uses harmonic continuum elasticity theory (i.e. insert Eqs. (4)–(6) into Eq. (11)). However, we have already seen evidence of anharmonic elastic effects in Ni–Au. Thus, we have performed LDA calculations of $q(a_\perp, \hat{k})$ directly from its definition in Eq. (2), rather than using the harmonic approximation in Eq. (6). In Fig. 1, we show the results of the LAPW calculations of $q^{\mathrm{Ni}}(a_\perp, \hat{k})$ and $q^{\mathrm{Au}}(a_\perp, \hat{k})$ for six principal directions: (100), (111), (110), (201), (311) and (221). It is clear that the calculated values of q are not independent of $a_\perp$, but rather show a marked

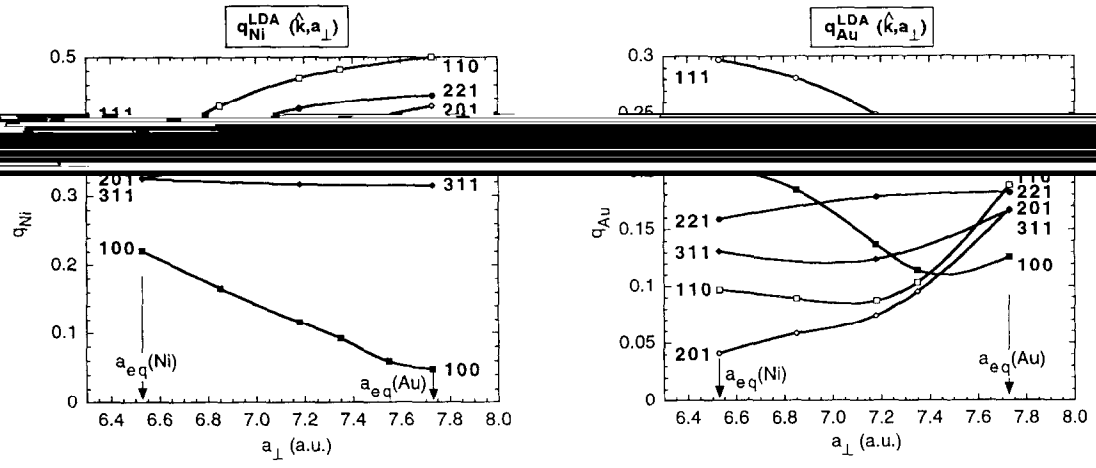

Fig. 1. LAPW calculations of $q^{(\lambda)}(a_\perp, \hat{k})$ of Eq. (2) for Ni–Au. Shown are (a) q^{Ni} and (b) q^{Au} for six principle directions.

value of $q^{Ni}(a_\perp, 100)$ is quite low upon expansion, indicating that Ni is elastically extremely soft in this direction. Au, on the other hand, becomes softest in the (201) direction for significant compression. In a separate publication [36], we will demonstrate that the anharmonic effects can be cast analytically in terms of the harmonic expressions of Eq. (4) by extending the expansion of $\gamma(\hat{k})$:

$$\gamma(\hat{k}) = \sum_L a_L(a_\perp) K_L(\hat{k}) \qquad (15)$$

to include angular momenta $L = 6$, 8 and 10 with the coefficients $a_L(a_\perp)$ obtained from LDA calculations rather than the $L = 0$, 4 expression of Eq. (6) used before [25].

used to numerically minimize Eq. (11) and hence to find $\Delta E_{CS}^{qs}(\hat{k}, x)$. The results for the CS energies are shown in Fig. 2. Here, also, the anharmonic effects

tries of the various directions are not all the same (effects which could not occur in the harmonic model). The most prominent feature of $\Delta E_{CS}^{eq}(\hat{k}, x)$

direction. Ni being soft and Au being relatively hard along (100) leads to Ni(Au) being highly distorted

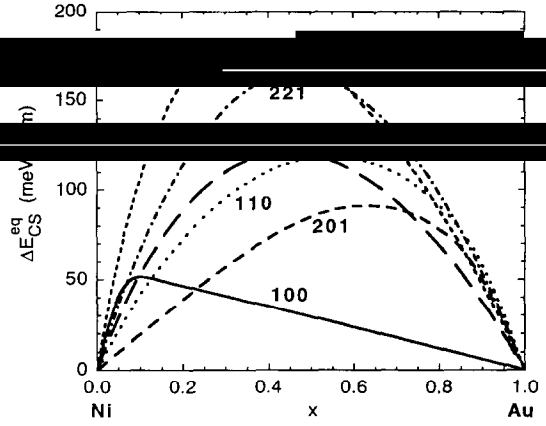

Fig. 2. LAPW calculations of $\Delta E_{CS}(\hat{k}, x)$ for Ni–Au for six principle directions.

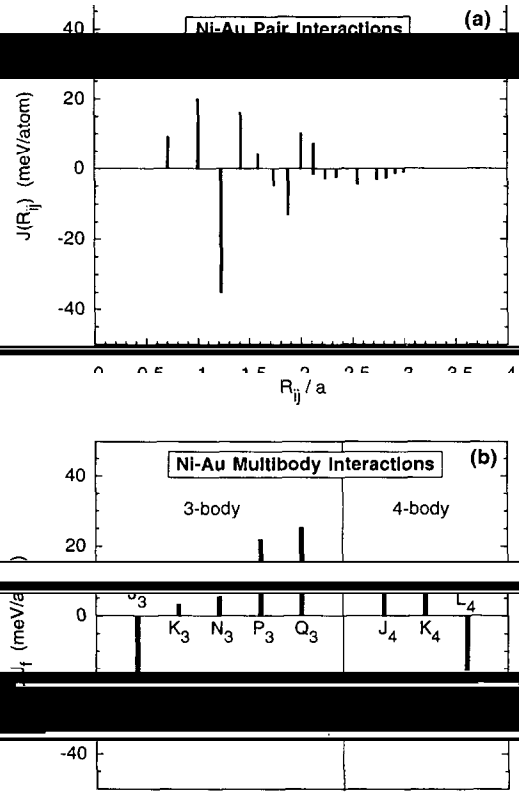

Fig. 3. (a) Pair and (b) multibody interaction energies for Ni–Au.

(101), K_3; (110), (200), N_3; (200), (002), P_3; (110), (103), Q_3; (110), (220), J_4; (110), (101), (011), K_4; (110), (101), (200) and L_4; (110), (101), (211).

(nearly undistorted) for long-period (100) Ni–Au

in $\Delta E_{CS}^{eq}(100, x)$ towards the Ni-rich compositions. Similar arguments can be applied to explain the opposite asymmetry of the (201) strain.

For E_{ref} to be useful in the k-space CE, one must be able to know this energy for all directions, not merely the ones for which it was calculated. To obtain such a useful form, we fit the constituent strain results of Fig. 2 to a series of Kubic harmonics (0–10th order) consistent with cubic symmetry (L = 0, 4, 6, 8, 10). This procedure provides not only a good fit of the calculated strain data, but also an analytic form to obtain the values of $\Delta E_{CS}^{eq}(\hat{k}, x)$ for all directions.

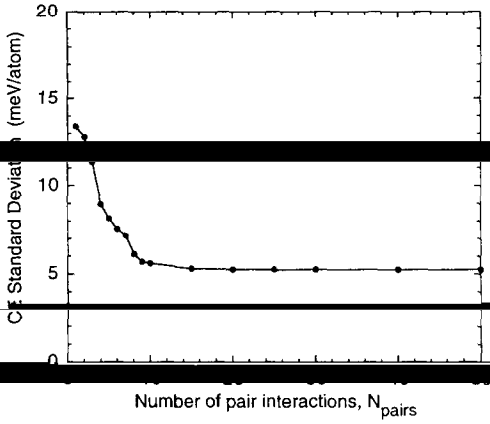

Fig. 4. Cluster expansion fitting error in Ni–Au versus the number of pair interactions included in the fit.

3.4. Stability of the cluster expansion

Using the calculated formation energies $\{\Delta H_\sigma\}$ (Table 3) and the anharmonic CS strain energy (Fig. 8), [illegible] 20 pair, 5 triplet and 5 quadruplet interactions. The standard deviation of the fitted energies relative to their LAPW values is 5.3 meV/atom, which is the same order of magnitude as the numerical uncertainties in LAPW. The results for pair and multibody interactions are shown in Fig. 3.

In order for the expansion to have a useful predictive capability, tests must be performed to assess the stability of the fit.

3.4.1. Changing the number of interactions

We performed tests of the stability of the fit with respect to the number of pair interactions, N_{pairs} = [illegible] included. It is clear that the fit is well converged for $N_{pairs} = 20$. We also tested the stability of the fit with respect to inclusion of more multibody interactions than are shown in Fig. 3. Including three additional triplet figures in the fit resulted in no change of the standard deviation of the fit, the added interactions had values < 2 meV/atom and the original interactions were changed by less than 2 meV/atom. Thus, the fit is stable with respect to the figures included (both pair and multibody).

3.4.2. Changing the number of structures

We also performed tests of the predictive ability of the fit by removing some structures from the fit. First, we removed three structures which were originally fit with small [illegible] moving these structures from the input set resulted in their energies changing by $\lesssim 1$ meV/atom. However, a much more critical test of the fit is to remove the structures which are fit most poorly: $SQS14_a$ and $SQS14_b$. Removing these structures from the fit changes their energies by only ~ 2–3 meV/atom. [illegible] fit is both stable and predictive.

4. Results of current calculations

4.1. Mixing enthalpy: How good are previous calculations?

Using the *k*-space cluster expansion in combination with a mixed real (reciprocal) space Monte Carlo [illegible] properties of Ni–Au alloys. Fig. 5 shows the mixing enthalpy as a function of temperature, $\Delta H_{mix}(T)$. Monte Carlo calculations were performed for a $16^3 = 4096$ atom cell, with 100 Monte Carlo steps per site for averages. The simulation was started at an extremely high temperature, and slowly cooled down using a simulated annealing algorithm. Also shown

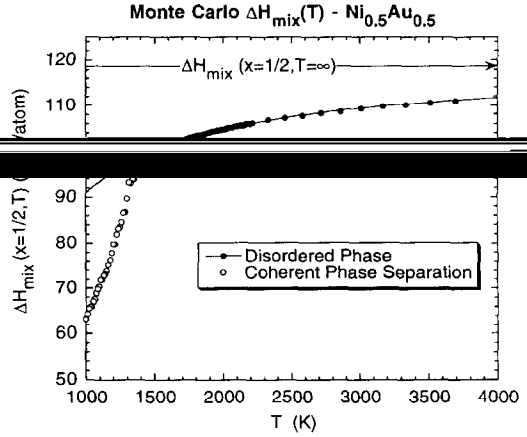

Fig. 5. $\Delta H(T)$ computed for $Ni_{0.5}Au_{0.5}$ from a combination of the *k*-space cluster expansion and Monte Carlo simulations.

completely random alloy. The difference between the Monte Carlo calculated $\Delta H_{mix}(T)$ and the random

$\Delta H_{mix}(T)$ to linear and quadratic functions of $\beta = 1/k_B T$ to extrapolate the values down in temperature below the point at which coherent phase separa-

where this quantity has been experimentally measured. These results are tabulated in Table 4, which shows both the effects of atomic relaxation (~ 100 meV/atom) and SRO (~ 25 meV/atom) on the mixing enthalpy and compares the value of atomically relaxed and short-range ordered mixing energy with those values from experiment. One can see that by taking into account *both* relaxation and SRO, LDA produces a value for the mixing energy which differs from experiment by only 15–20 meV/atom. Thus, we conclude from this comparison that high quality LDA calculations provide accurate energetics for the Ni–Au system.

The preceding discussion leads to a number of conclusions regarding previous calculations of ΔH_{mix}:

(i) Since relaxation reduces ΔH_{mix} by ~ 100 meV/atom, the unrelaxed ΔH_{mix} values ('*d*' in

meV/atom, the results of previous calculations that

Table 4
ΔH_{mix} for $Ni_{0.5}Au_{0.5}$. All energies in meV/atom. SQS-4 refers to a 4-atom special quasi-random structure ($Y2$). This table shows the effects of relaxation (first line minus second line) and short-range order (third line minus fourth line) on the mixing energy

SQS-4 unrelaxed ($T = \infty$)	+192
CE relaxed ($T = 1100$ K)	+93
Expt. (calorimetry) $T = 1150$ K	+76

omitted SRO (all except '*t*' in Table 1) have to be adjusted accordingly.

(iii) In light of the fact that the empirical potential-

full-potential LDA methods for unrelaxed, ordered compounds (Table 2), the results of *relaxed, mixing energies of random alloys* appear to be questionable

one can find the configurational entropy of the $Ni_{0.5}Au_{0.5}$ disordered phase by integrating the energy down from infinite temperature (where the configurational entropy is known):

$$\Delta S(T) = \Delta S(T=\infty) + E(T)/T - k_B \int_0^\beta E(\beta)\, d\beta \quad (14)$$

The configurational entropy obtained from thermodynamic integration in this way is

$$\Delta S_{conf}(Ni_{0.5}Au_{0.5}, T = 1100\ K) = 0.56 k_B, \quad (15)$$

compared to the 'ideal' (infinite temperature) value of

$$\Delta S_{conf}(Ni_{0.5}Au_{0.5}, T \to \infty) = 0.69 k_B, \quad (16)$$

This calculated value for the *configurational* entropy of mixing can be compared with the experimentally measured values of *total* entropy of mixing: Calori-

the *non-configurational* entropy and find it to be large: $\Delta S_{non\text{-}conf}(T \sim 1100\ K) = 1.04 - 0.56 = 0.48 k_B$. This non-configurational entropy is hence responsible for T_{MG} being so small experimentally, compared to all the theoretical results. In fact, if we use the calculated $\Delta H_{mix} = 93$ meV/atom and the combined 'experimental/calculated' $\Delta S_{non\text{-}conf} = 0.48 k_B$ in the following formula:

k_B + $\Delta S_{non\text{-}conf}$

much closer to the experimental values (T_{MG} 1065 K and $k_B T_{MG}/\Delta H_{mix} = 1.2$) than using the above formula neglecting non-configurational entropy (T_{MG} ~ 2150 K and $k_B T_{MG}/\Delta H_{mix} = 2.0$).

From this consideration of non-configurational effects, one should conclude that the accuracy of a calculation with configurational degrees of freedom only (as is done in most of the previous calculations [4]), should be determined by looking at

temperatures do so precisely because they have "bad energetics.

4.3. Short-range order of $Ni_{1-x}Au_x$ solid solutions

$Ni_{1-x}Au_x$ alloys. We show the results of our SRO

atoms was used, with 100 Monte Carlo steps for

quent 500 steps. Several calculations and measurements of the SRO exist in the literature: Wu and Cohen [2] used diffuse X-ray scattering to deduce the atomic SRO of $Ni_{0.4}Au_{0.6}$ at $T = 1023$ K. The measured diffuse intensity due to SRO must be separated from all the other contributions which give rise to diffuse intensity and for this purpose Wu and Cohen used 25 real-space Fourier shells of SRO parameters, and found the rather surprising result that the peak intensity in reciprocal space due to SRO is of ordering-type and occurs at the point $\boldsymbol{k}_{SRO} = (0.6, 0, 0)$, rather than $\boldsymbol{k}_{SRO} = (0, 0, 0)$ which would be ex-

Lu and Zunger [8] calculated the SRO (using 21 real-space shells) and found peaks at $\boldsymbol{k} = (0.8, 0, 0)$ whereas Asta and Foiles [20] used an embedded atom method and found the SRO (using 8 real-space shells) to peak at $\boldsymbol{k} = (0.5, 0, 0)$. Our calculations for the SRO of $Ni_{0.4}Au_{0.6}$ are given in Fig. 6. We have

bility gap temperature for our alloy Hamiltonian. We find that, using 8, 25 and 100 shells, the SRO peaks at (0.65, 0, 0), (0.40, 0, 0) and (0.38, 0, 0) respectively, in good agreement with both the measurements of Wu and Cohen ($\boldsymbol{k}_{SRO} = (0.6, 0, 0)$ for 25 shells) and also with previous calculations.

Eq. (12) shows that the alloy Hamiltonian used in

action terms, and the constituent strain terms. It is interesting to see the effect of each of these portions of the alloy Hamiltonian on SRO. Thus, in addition to the 'full' calculations, which contain pairs, multibodies and constituent strain in the alloy Hamilto-

interactions. These results are shown in Fig. 7. (Be-

required to converge the SRO of CS alone; thus we

Fig. 7.) One can see that the SRO with CS only is dominated by almost constant streaks of intensity along the $\Gamma - X$ line and very little intensity elsewhere. This SRO pattern is understandable when one considers that the constituent strain at this composition (Fig. 2) is much softer (much lower in energy) in the (100) direction than along any other direction. Thus, (100)-type fluctuations in the random alloy are energetically favored, and because the constituent strain is dependent only on direction and not on the length of the wavevector, one should expect that all fluctuations along the (100) directions will occur

Contrasting this SRO using CS only with that calculated using both CS energy and pair interactions (but not multibody interactions) shows that the pair interactions create a peak in intensity along the $\Gamma - X$ line, but significantly closer to Γ than the peak intensity using the 'full' alloy Hamiltonian. Thus,

Γ point, the multibody interactions move this peak out from Γ towards the X-point.

4.4. Standard inverse Monte Carlo would give unphysical interaction energies: A challenge

The statistical problem we have solved here involves the calculation of the alloy SRO at high temperature for given alloy Hamiltonian ($\{J_{ij}\}$, $\{J_f\}$

[4] Some of the previous calculations (f, i, j of Table 1) estimated the effects of vibrations on the phase diagram, either using a simple Debye model (f) with LDA bulk modulus calculations or continuous-space Monte Carlo simulations (i, j) using the elastic response of an empirical potential.

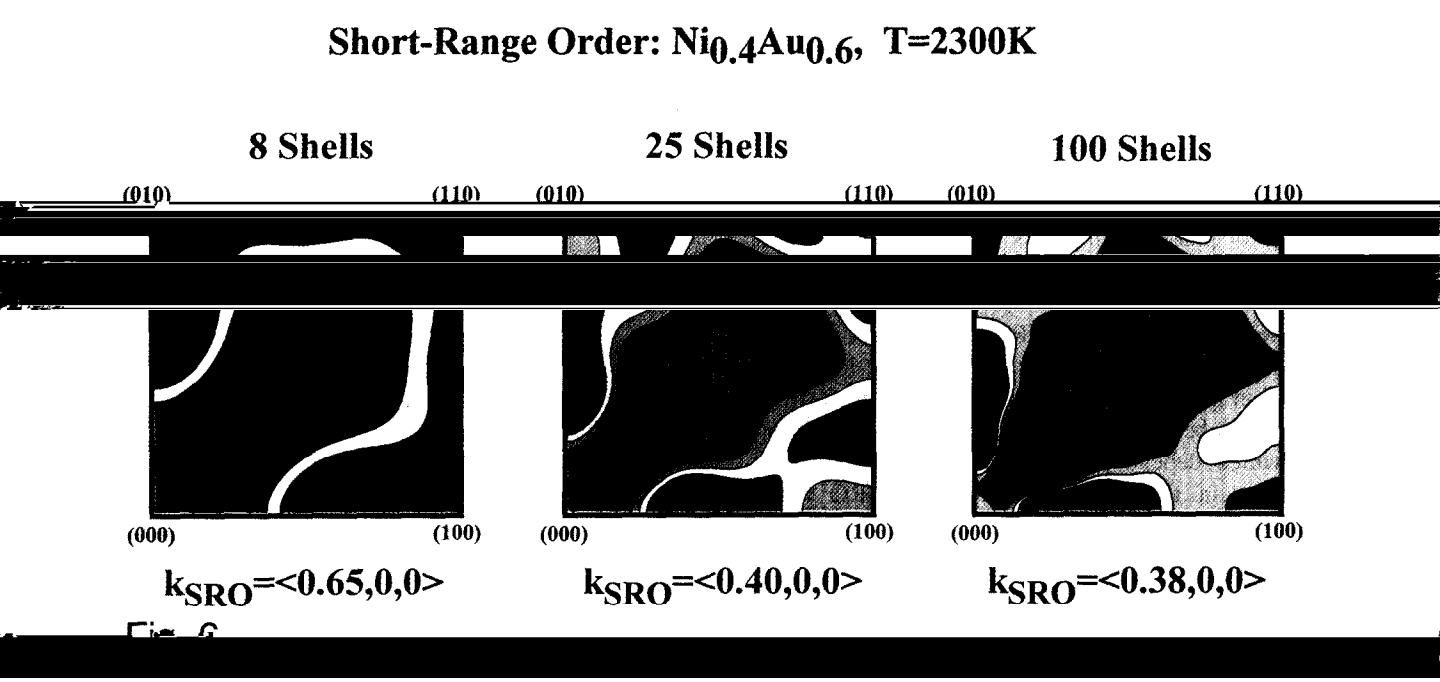

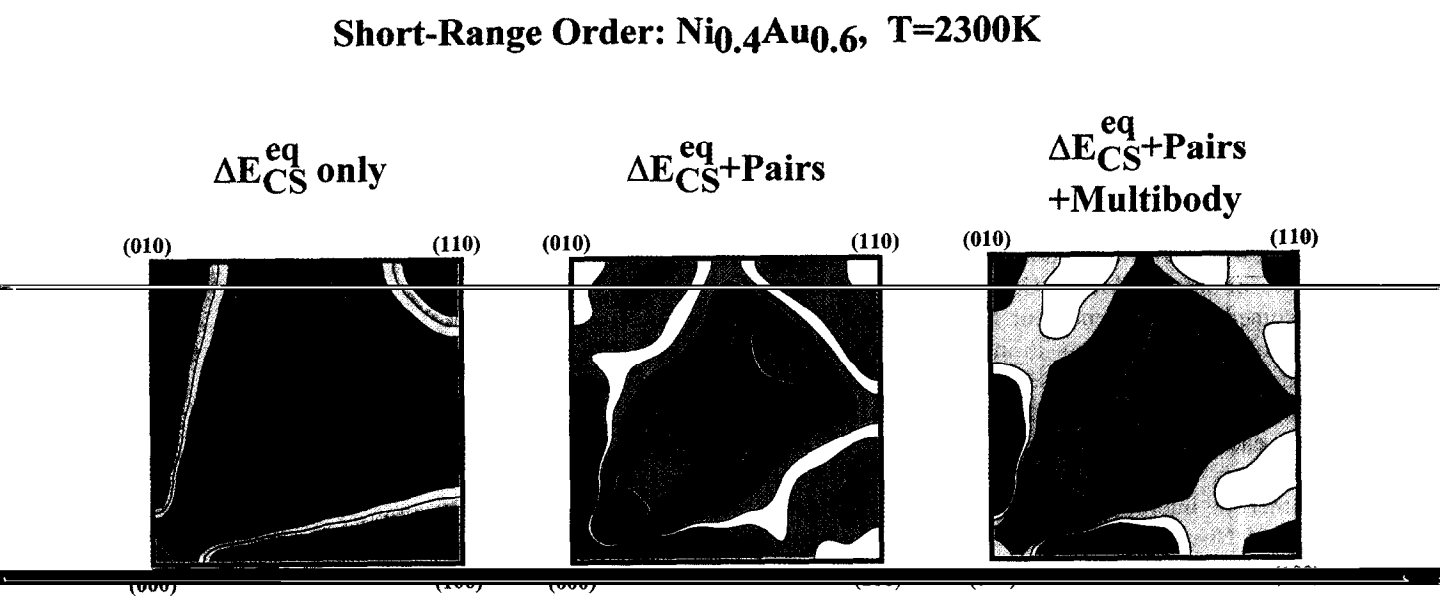

Fig. 7

Fig. 6. Monte Carlo-calculated short-range order of $Ni_{0.4}Au_{0.6}$ in the ($hk0$) plane using (a) 8, (b) 25 and (c) 100 shells of Warren Cowley SRO parameters. The peak intensity is the red shaded contour while the lowest contours are shaded blue. Contours are separated by 0.1 Laue unit in each plot.

and ΔE_{CS}). However, a popular technique used to study phase stability in alloys involves the 'inverse' problem of determining a set of pair-only interactions $\{\tilde{J}_{ij}\}$ from a measured or calculated SRO pattern and the subsequent use of these pair interactions to determine thermodynamic properties other than the SRO. In fact, $\{\tilde{J}_{ij}\}$ are often used to determine ΔH_{mix} of phase stability. As we have mentioned in [illegible] on energy terms that are SRO-independent e.g. the vents, in principle, the interactions deduced from SRO from being applied to predict physical properties which depend on $G(x)$, such as ΔH_{mix}. For example, in the case of Ni–Au, the SRO is of ordering type. Thus, we expect that inverting the SRO of Ni–Au (e.g. via inverse Monte Carlo) would produce interactions $\{\tilde{J}_{ij}\}$ which are of ordering type and using these interactions to predict the mixing enthalpy would result in the unphysical result $\Delta H_{mix} < 0$.

One might suggest that by changing the temperature, one could obtain a shift of the SRO from ordering to clustering type, and thus the inverse [illegible] correctly give $\Delta H_{mix} > 0$. However, we have computed the SRO for several temperatures, and find no evidence of a shift in SRO to clustering type.

A test of our expectations by any of the practitioners of inverse Monte Carlo would certainly be welcomed. To that end, our SRO calculations are [illegible] extract interactions. These SRO calculations are available for a variety of compositions and temperatures, each with a large number of real-space SRO parameters. It would be of great interest to see whether the interactions extracted from inverting the SRO of Ni–Au would produce the correct sign of ΔH_{mix}.

Acknowledgements

[illegible] Research (OER), Division of Materials Science of the Department of Energy, under contract No. DE-AC36-83CH10093. The authors would like to thank Dr. M. Asta for providing the EAM values in Table 2 and Mr. D. Morgan for communicating his results to us prior to publication.

References

[illegible]
1963.
[2] T.B. Wu, J.B. Cohen, Acta Metall. 31 (1983) 1929.
[illegible]
[4] B. Golding, S.C. Moss, B.L. Averbach, Phys. Rev. 158 (1967) 637.
[5] T.B. Wu, J.B. Cohen, W. Yelon, Acta Metall. 30 (1982) 2065.
[6] T.B. Wu, J.B. Cohen, Acta Metall. 32 (1984) 861.
[7] H.E. Cook, D. de Fontaine, Acta Metall. 17 (1969) 915.
[8] Z.-W. Lu, A. Zunger, Phys. Rev. B 50 (1994) 6626.
[9] L.G. Ferreira, A.A. Mbaye, A. Zunger, Phys. Rev. B 37 (1988) 10547.
[10] V. Gerold, J. Kern, Acta Metall. 35 (1987) 393.
[11] W. Schweika, H.-G. Haubold, Phys. Rev. B 37 (1988) 9240.
[12] L. Reinhard, B. Schönfeld, G. Kostorz, W. Bührer, Phys. [illegible]
[illegible] C.J. Sparks, Phys. Rev. B 45 (1992) 2662.
[illegible]
[15] T. Deutsch, A. Pasturel, in: A. Gonis, P. Turchi, J. Kudrnovsky (Eds.), Stability of Materials, NATO-ASI Series, Plenum, 1996.
[16] C. Amador, G. Bozzolo, Phys. Rev. B 49 (1994) 956.
[17] C. Colinet, J. Eymery, A. Pasturel, A.T. Paxton, M. van Schilfgaarde, J. Phys. 6 (1994) L47.
[illegible]
5792.
[20] M. Asta, S.M. Foiles, Phys. Rev. B 53 (1996) 2389.
[21] R. Tetot, A. Finel, in: A. Gonis, P. Turchi, J. Kudrnovsky (Eds.), Stability of Materials, NATO-ASI Series, Plenum, 1996.
[22] J. Eymery, F. Lancon, L. Billard, J. Phys. Paris 3 (1993) 787.
[23] J.W.D. Connolly, A.R. Williams, Phys. Rev. B 27 (1983) 5169.
[24] D. de Fontaine, Solid State Phys. 34 (1979) 73.
[25] D.B. Laks, L.G. Ferreira, S. Froyen, A. Zunger, Phys. Rev. B [illegible]
[26] A. Zunger, in: P.E.A. Turchi, A. Gonis (Eds.), Statistics and [illegible]
[27] C. Wolverton, A. Zunger, Phys. Rev. B 50 (1994) 10548.
Growth, vol. 3, Elsevier, 1994.

[30] J.E. Bernard, A. Zunger, Appl. Phys. Lett. 65 (1994) 16527.
[31] M. Asta, private communication.
[32] D.J. Singh, Planewaves, Pseudopotentials and the LAPW Method, Kluwer, Boston, 1994.
[33] E. Wigner, Phys. Rev. 46 (1934) 1002.
[34] S. Froyen, Phys. Rev. B 39 (1989) 3168.
[35] A. Zunger, S.-H. Wei, L.G. Ferreira, J.E. Bernard, Phys. Rev. Lett. 65 (1990) 352.
[36] V. Ozoliņš, C. Wolverton, A. Zunger, to be published.
[37] C. Wolverton, A. Zunger, B. Schonfeld, Solid State Commun. 101 (1997) 519.